Supporting Information

Strengthening the magnetic interactions in pseudobinary first-row transition metal thiocyanates, M(NCS)$_2$

Euan N. Bassey,[1] Joseph A. M. Paddison,[2,3,4] Evan N. Keyzer,[1] Jeongjae Lee,[1,5] Pascal Manuel,[6] Ivan da Silva,[6] Siân E. Dutton,[3] Clare P. Grey[1,*] and Matthew J. Cliffe[1,7,*]

[1]Department of Chemistry, Lensfield Road, University of Cambridge, CB2 1EW, United Kingdom

[2]Churchill College, University of Cambridge, Storey's Way, Cambridge, CB3 0DS, United Kingdom

[3]Cavendish Laboratory, Department of Physics, University of Cambridge, JJ Thompson Avenue, Cambridge, CB3 0HE, United Kingdom

[4]Materials Science & Technology Division, Oak Ridge National Laboratory, Oak Ridge, TN 37831, United States of America

[5]School of Earth and Environmental Sciences, Seoul National University, Seoul 08826, Korea

[6]ISIS Facility, STFC Rutherford Appleton Laboratory, Harwell Oxford, Didcot, OX11 0QX, United Kingdom

[7]School of Chemistry, University Park, Nottingham, NG7 2RD, United Kingdom

* To whom correspondence should be addressed;
E-mail: cpg27@cam.ac.uk; matthew.cliffe@nottingham.ac.uk

Contents

List of Figures

List of Tables

1. Synthesis of *M*(NCS)₂ (*M* = Mn, Fe, Co and Ni)

Mn(NCS)₂

$MnSO_4 \cdot H_2O$ (Sigma Aldrich, 99%, 1.690 g, 10.00 mmol) was dissolved in the minimum volume of deionised H_2O to yield a pale pink solution. A saturated solution of $Ba(SCN)_2 \cdot 3H_2O$ (Alfa Aesar, 98%, 3.075 g, 10.00 mmol) was added to this in portions, forming a white precipitate immediately. The reaction mixture was stirred overnight and the precipitate isolated by centrifugation and then decanting the supernatant liquor. The solvent was removed *in vacuo* to yield a yellow residue, which was dried by heating in air at 120°C for one hour before further drying under dynamic vacuum for 48 hours at 100°C. Manganese (II) thiocyanate (1.460 g, 6.01 mmol, 60%) was collected as a pale yellow microcrystalline powder. The same procedure—with all quantities scaled up by a factor of 6.5—was used to synthesise the sample used for neutron diffraction measurements. This compound readily hydrates in ambient humidity, turning from pale yellow to green; as such, it was stored in a dry argon atmosphere.

The product was analysed for elemental purity (combustion analysis for CHN). Found (calculated) $C_2N_2S_2Mn$: C 13.32% (14.04%), H 0.05% (0.00%), N 15.32% (16.37%).

Fe(NCS)₂

KSCN (Sigma Aldrich, 99%, 0.117 g, 1.2 mmol) was dissolved in dry acetonitrile (approximately 20 cm^3) and the clear colourless solution stirred under a nitrogen atmosphere at room temperature. The solution was added to $Fe(BF_4)_2 \cdot 6H_2O$ (Aldrich, 97%, 0.203 g, 0.6 mmol), instantly forming a dark red solution. The reaction mixture was stirred under a nitrogen atmosphere at room temperature for approximately five minutes, separating to a dark red solution and white precipitate (coloured red by the strongly-coloured supernatant liquor). The mixture was filtered *via* a cannula and the supernatant liquor taken to dryness *in vacuo* to yield a dark red-purple residue, which was heated under dynamic vacuum to form an orange-brown powder. Iron(II) thiocyanate (0.047 g, 0.27 mmol, 45%) was isolated as an orange-brown microcrystalline powder. The same procedure—with all reagent masses scaled up by a factor of 33—was used to synthesise the sample used for neutron diffraction measurements. The compound is air sensitive, oxidising to form a dark brown powder; as such, the compound was stored under inert atmosphere.

The product was analysed for elemental purity (combustion analysis for CHN). Found (calculated) $C_2N_2S_2Fe$: C 13.60% (13.97%), H 0.10% (0.00%), N 15.39% (16.29%).

Co(NCS)₂

$CoSO_4 \cdot 7H_2O$ (Sigma Aldrich, 99%, 2.811 g, 10.00 mmol) was dissolved in the minimum volume of deionised H_2O to generate a clear red solution. A saturated solution of $Ba(SCN)_2 \cdot 3H_2O$ (Alfa Aesar, 98%, 3.075 g, 10.00 mmol) in deionised H_2O was added in portions, instantly forming a white precipitate, coloured by the strong red supernatant liquor. The reaction mixture was left to stir at room temperature overnight, and the precipitate isolated by centrifugation and then decanting the supernatant liquor. The supernatant liquor was dried *in vacuo*, generating a red-brown residue, which was further dried by heating in air at approximately 120°C for one hour. Cobalt (II) thiocyanate (1.257 g, 7.18 mmol, 72%) was collected as a red-brown microcrystalline powder. The same procedure—with all quantities

scaled up by a factor of 6.5—was used to synthesise the sample used for neutron diffraction measurements.

Ni(NCS)$_2$

$NiSO_4 \cdot 6H_2O$ (Alfa Aesar, 99.97%, 2.628 g, 10.00 mmol) was dissolved in the minimum volume of deionised H_2O, forming a clear green solution. To this, a saturated solution of $Ba(SCN)_2 \cdot 3H_2O$ (Alfa Aesar, 98%, 3.075 g, 10.00 mmol) in deionised H_2O was added, instantly forming a white precipitate, coloured green by the supernatant liquor. The reaction mixture was stirred at room temperature overnight and the precipitate removed with a centrifuge. The liquor was dried *in vacuo* to generate a green-brown microcrystalline powder. Nickel (II) thiocyanate (1.501 g, 8.58 mmol, 86%) was collected as a green-brown microcrystalline powder. The same procedure—with all quantities scaled up by a factor of 6.5—was used to synthesise the sample used for neutron diffraction measurements.

2. Powder X-Ray Diffraction Results

An initial assessment of the bulk phase purity of each compound was carried out using powder X-ray diffraction. The diffraction patterns collected were analysed using Pawley[1] and Rietveld[2,3] refinements using the TOPAS Academic 6.0 software package.[4,5]
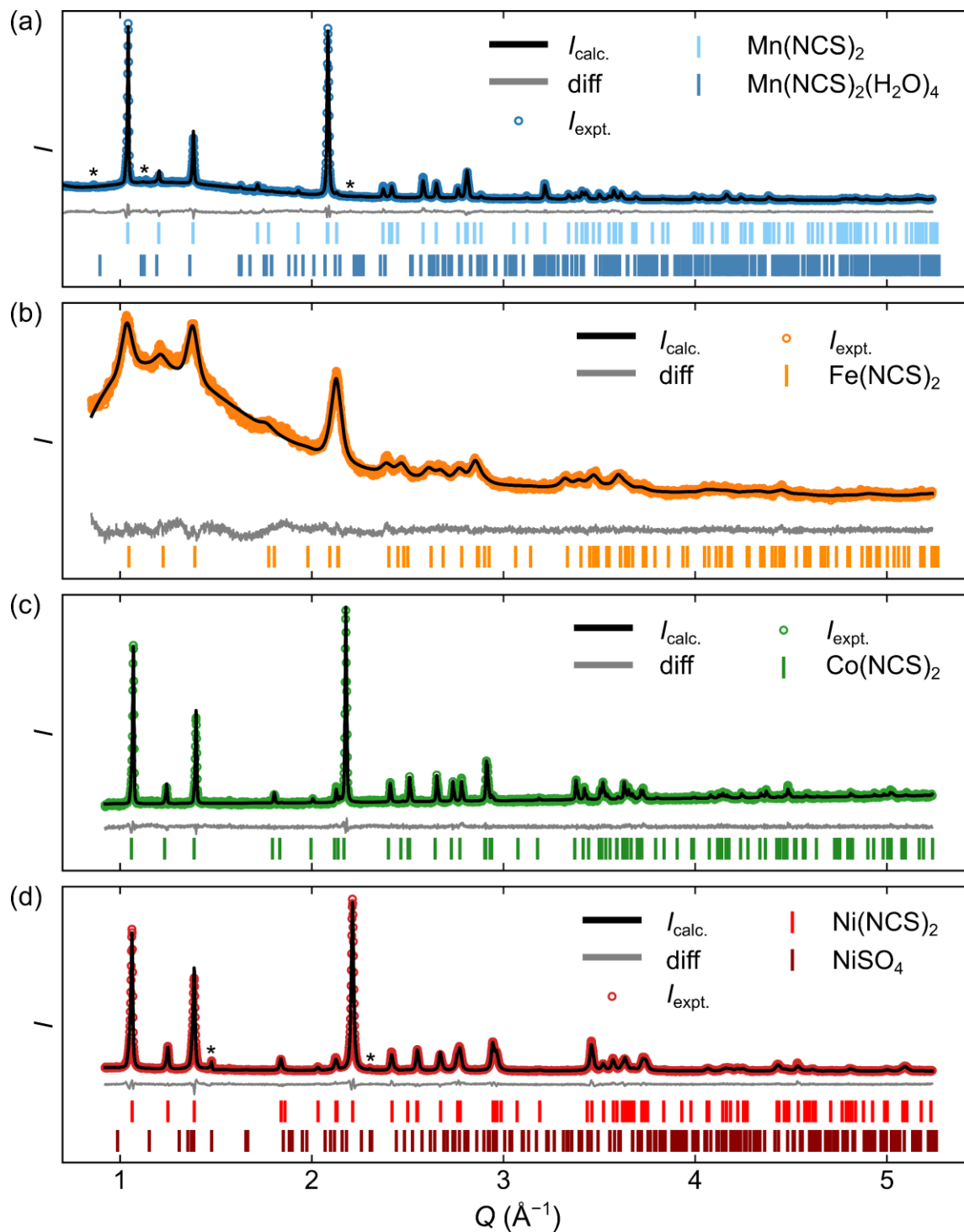
Figure S1. Powder X-ray diffraction patterns collected for **(a)** $Mn(NCS)_2$, **(b)** $Fe(NCS)_2$, **(c)** $Co(NCS)_2$ and **(d)** $Ni(NCS)_2$. Asterisks lie directly above reflections arising from impurity phases (either hydrates or unreacted starting material). The broad features near $Q = 1.2$ Å^{-1} for $Mn(NCS)_2$ and $Fe(NCS)_2$ correspond to diffuse scattering from the polyimide (Kapton) films used to encase these moisture- and air-sensitive samples.

3. Thermogravimetric Analysis Results

To assess whether solvent remained trapped in the synthesised frameworks, we carried out thermogravimetric analysis (TGA), as shown in Figure S2. The small loss in mass observed between $T = 50°C$ and approximately 300°C likely corresponds to the loss of surface adsorbed water on particles of the material [Figure S2(a)], consistent with the exotherm peaks observed over this temperature range [Figure S2(b)]. Beyond 400°C, the materials decompose, indicated by the sharp loss of mass.
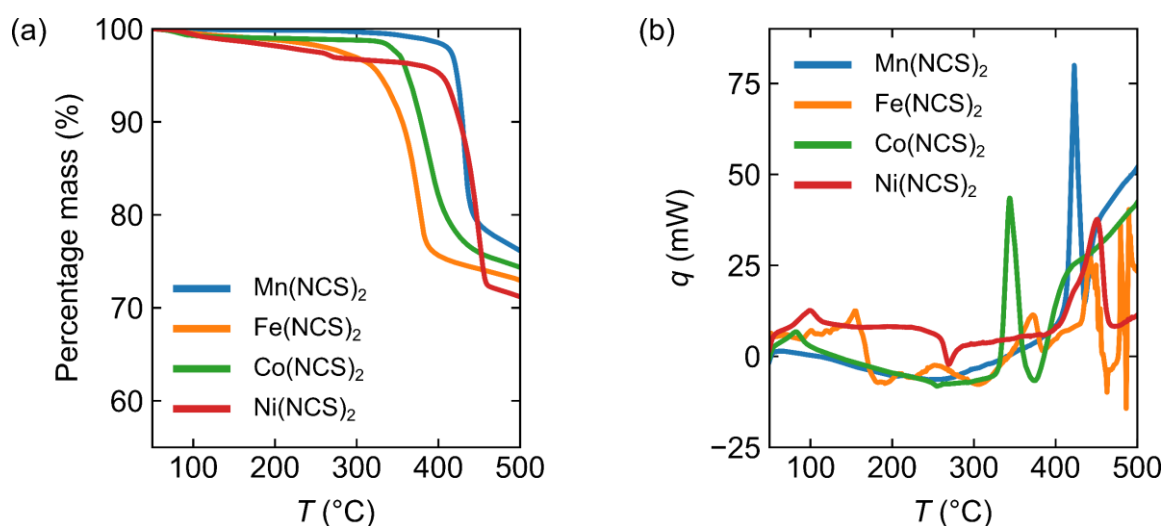
Figure S2. Thermogravimetric data collected for $M(NCS)_2$ (M = Mn, Fe, Co, Ni). **(a)** shows the percentage mass loss of material, relative to the initial mass of material, over the temperature range 50°C–500°C. **(b)** shows the change in heat flow, q, measured over the same temperature range for the same sample as in **(a)**. Data above 500°C have not been included, as the noise in the q significantly obscures the data.

4. Isothermal Magnetisation Results

To examine whether any field-induced magnetic phase transitions occur in $M(NCS)_2$ (M = Mn, Fe, Co, Ni), we carried out isothermal magnetisation measurements on each material [Figures S3–S6]. No such transitions could be identified; the inflections seen near H = 0 T for each compound in the −7 to +7 T field-swept measurements could not be definitively assigned.

Figure S3. Isothermal magnetisation data ($M(H)$ curves) collected for Mn(NCS)$_2$. **(a)** shows the $M(H)$ curves obtained over H = −0.01 to +0.01 T, with the corresponding variation in $\frac{dM}{dH}$ shown in **(c)**. **(b)** shows the $M(H)$ curves for the range H = −7 to +7 T, whilst **(d)** shows the corresponding variation in $\frac{dM}{dH}$.
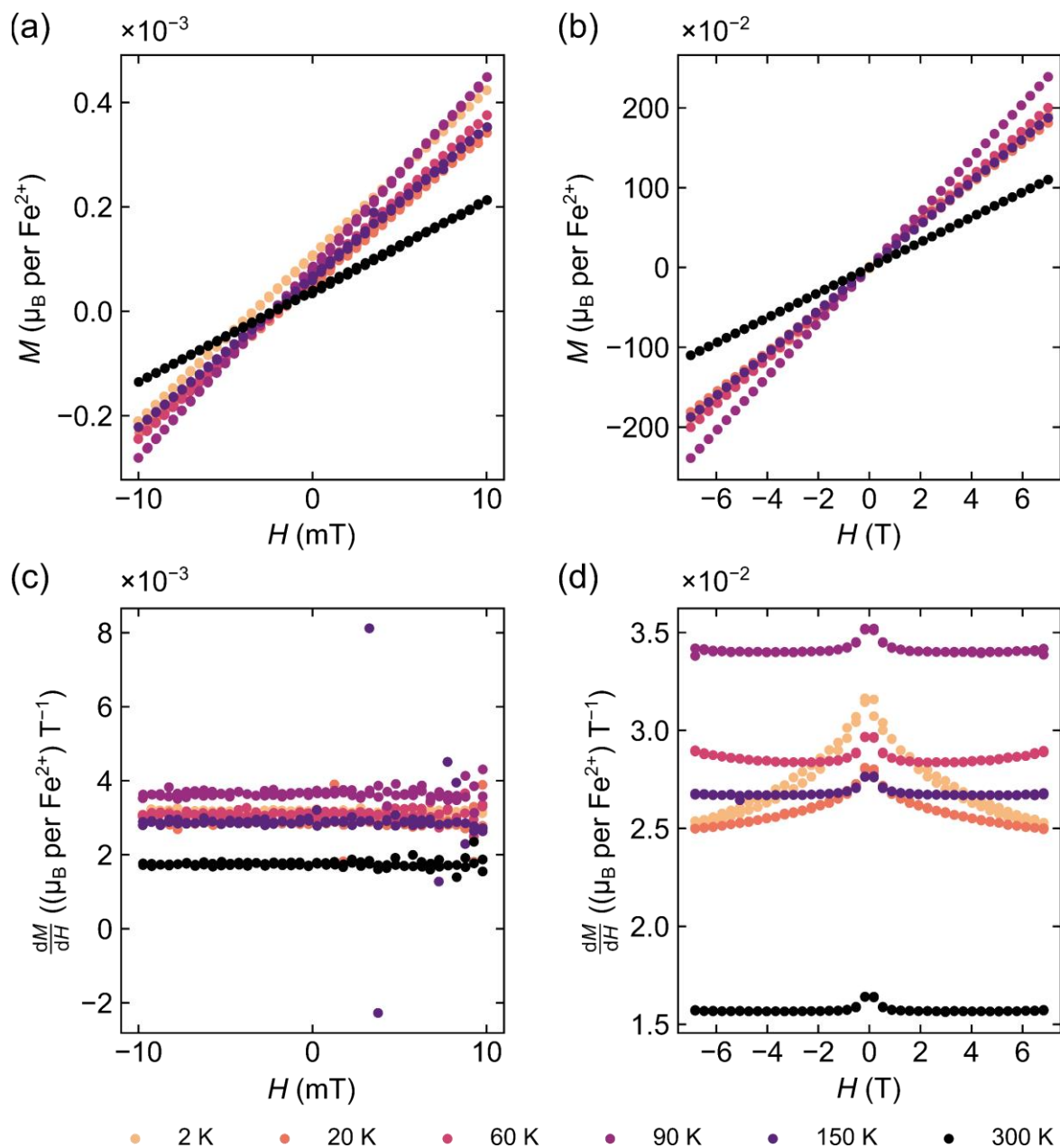
Figure S4. Isothermal magnetisation data ($M(H)$ curves) collected for Fe(NCS)$_2$. **(a)** shows the $M(H)$ curves obtained over $H = -0.01$ to $+0.01$ T, with $\frac{\mathrm{d}M}{\mathrm{d}H}$ over the same range shown in **(c)**. **(b)** shows the $M(H)$ curves for the range $H = -7$ to $+7$ T, whilst **(d)** shows the corresponding variation in $\frac{\mathrm{d}M}{\mathrm{d}H}$.
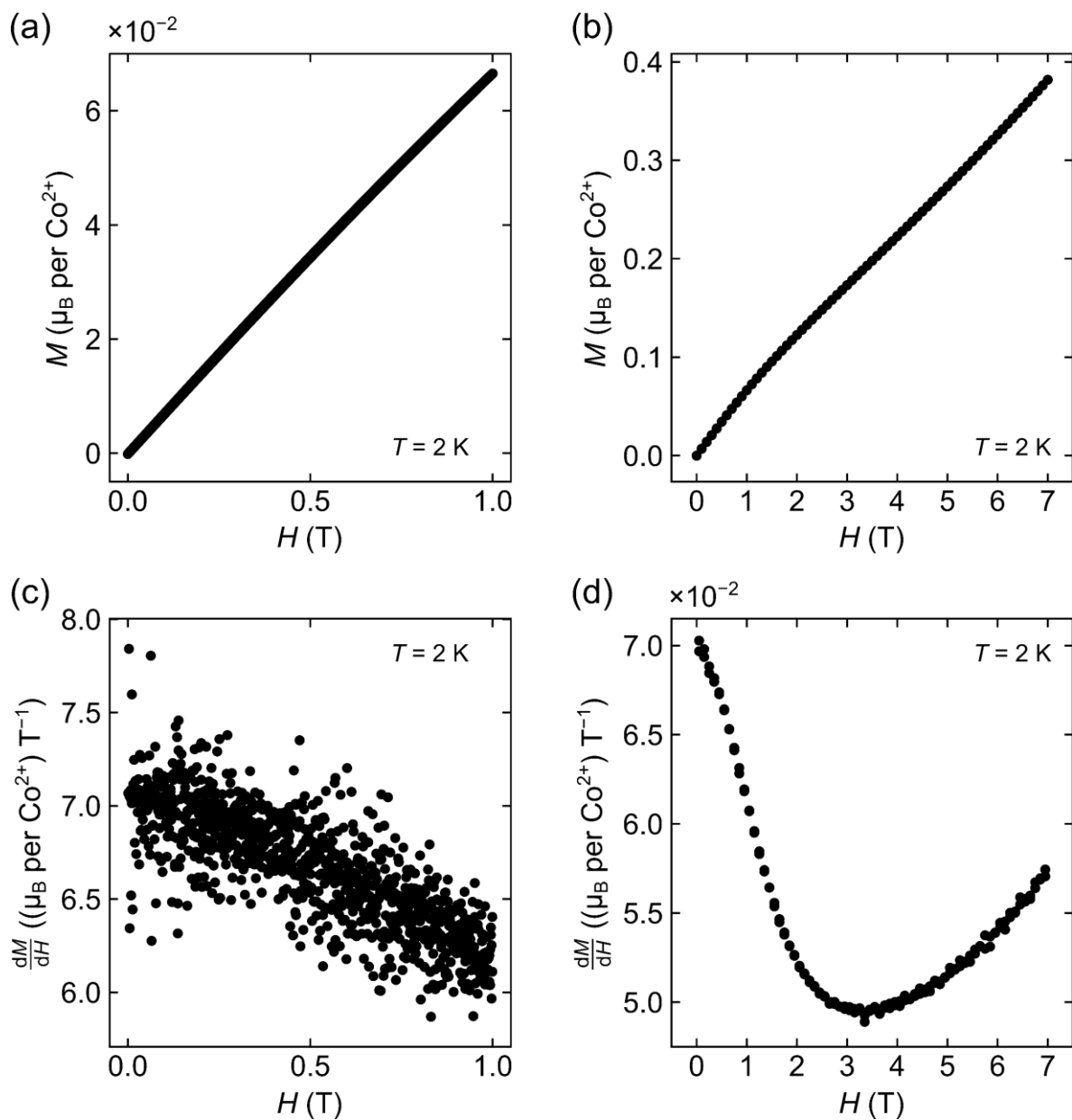
Figure S5. Isothermal magnetisation data ($M(H)$ curves) collected for Co(NCS)$_2$. **(a)** shows the $M(H)$ curve recorded between $H = 0$ to 1 T, with the corresponding variation in $\frac{dM}{dH}$ shown in **(c)**. **(b)** shows the $M(H)$ curves for the range $H = 0$ to 7 T, whilst **(d)** shows the corresponding variation in $\frac{dM}{dH}$.
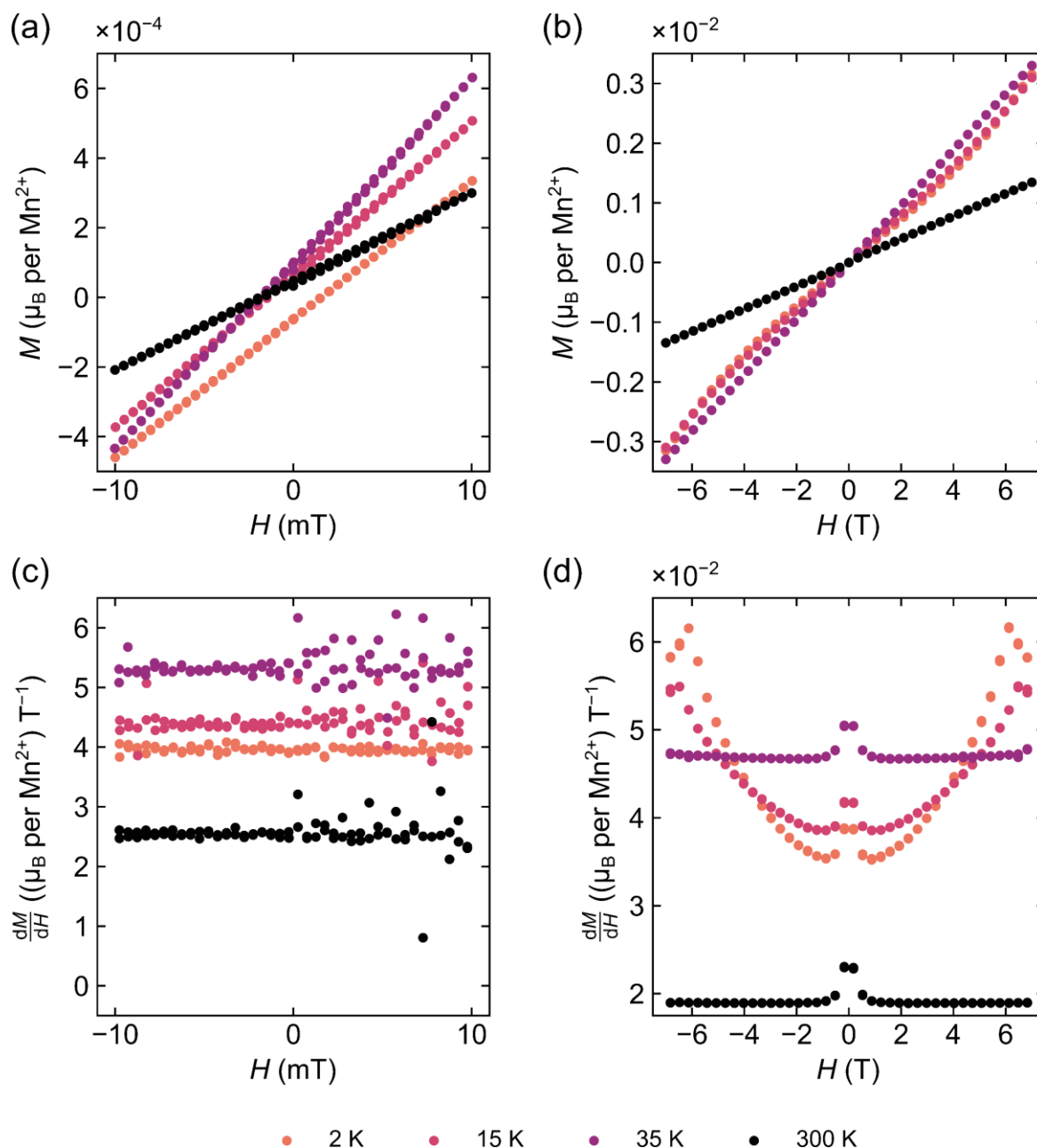
Figure S6. Isothermal magnetisation data ($M(H)$ curves) collected for Ni(NCS)$_2$. **(a)** shows the $M(H)$ curves obtained over $H = -0.01$ to $+0.01$ T, with the corresponding variation in $\frac{\mathrm{d}M}{\mathrm{d}H}$ shown in **(c)**. **(b)** shows the $M(H)$ curves for the range $H = -7$ to $+7$ T, whilst **(d)** shows the corresponding variation in $\frac{\mathrm{d}M}{\mathrm{d}H}$.
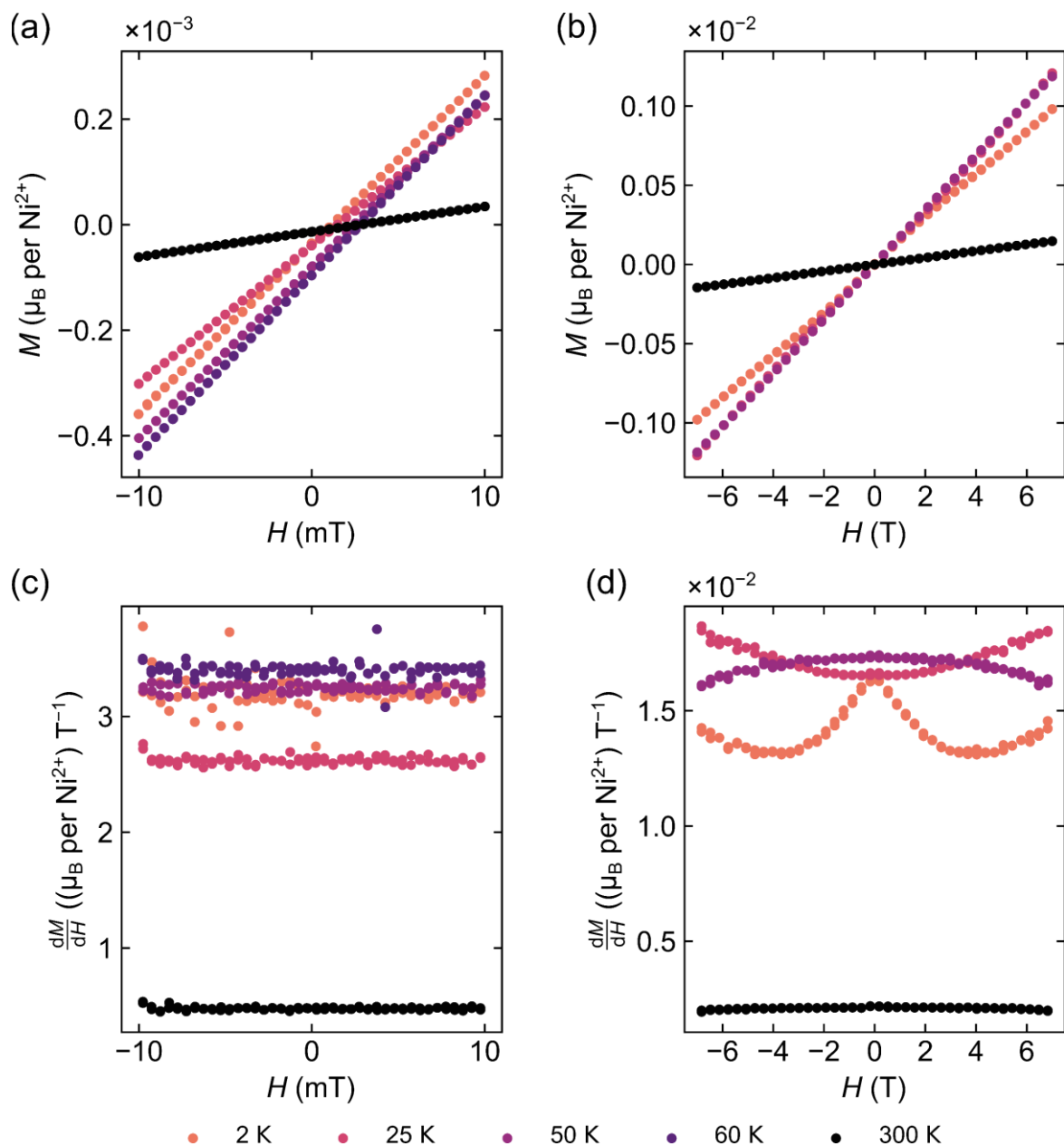
5. Zero-Field and Field Cooled Magnetic Susceptibility Results

Both the zero-field cooled (ZFC) and field cooled (FC) magnetic susceptibilities of M(NCS)$_2$ were recorded, to check for any deviations between the data sets and identify the presence of a net magnetic moment. None of the compounds show such a deviation; the small deviations seen at low temperatures are likely dominated by non-zero magnetic moments in paramagnetic impurities in each sample.

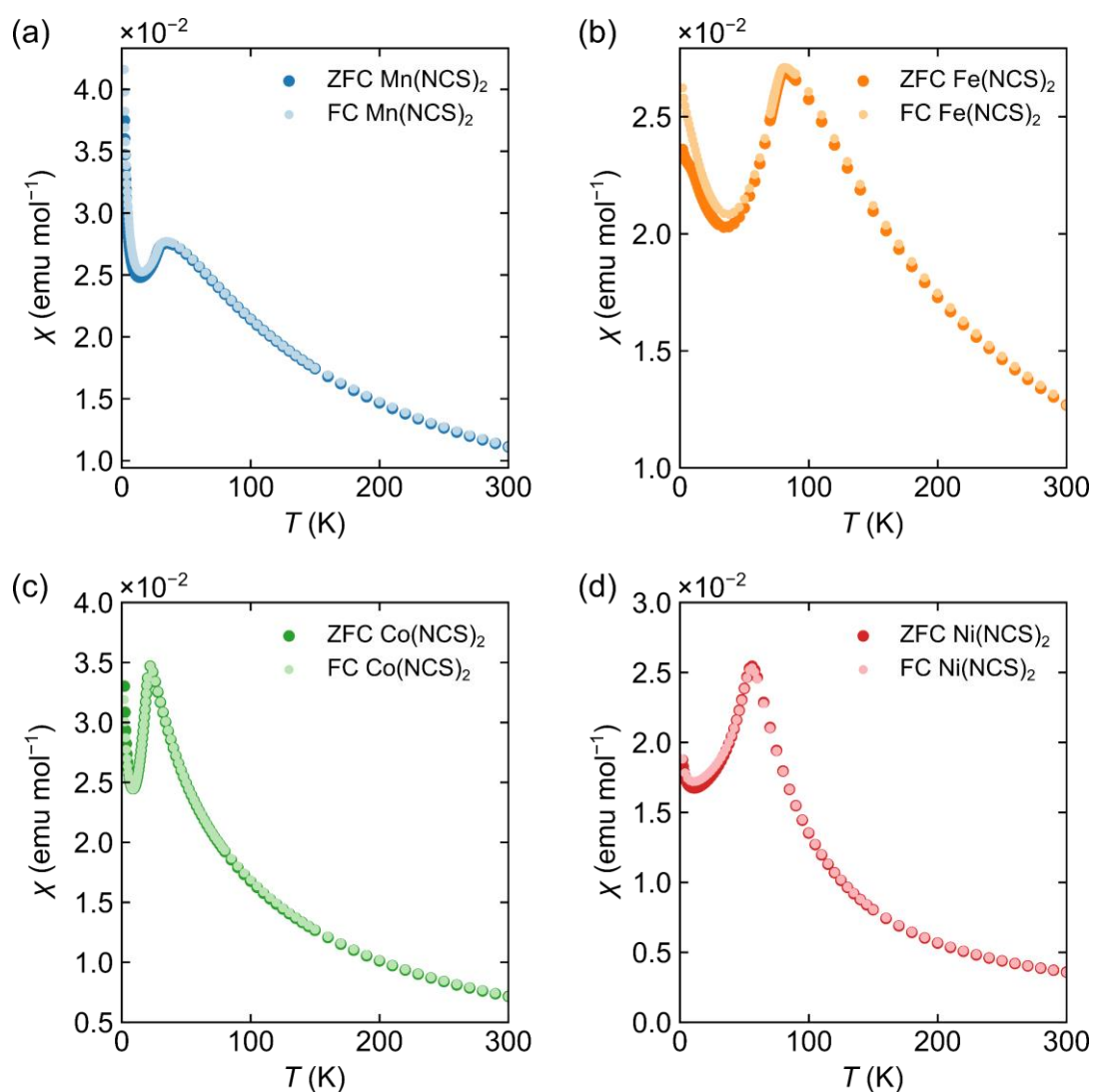**Figure S7.** Zero-field and field cooled (ZFC and FC, respectively) magnetic susceptibility data collected for for Mn(NCS)$_2$ (**a**), Fe(NCS)$_2$ (**b**), Co(NCS)$_2$ (**c**) and Ni(NCS)$_2$ (**d**) in a constant magnetic field strength H = 0.01 T. The markers for the FC data sets have been made smaller intentionally, to better identify any differences between the ZFC and FC susceptibilities.

6. Powder Neutron Diffraction Rietveld Fits

The powder neutron diffraction (PND) patterns recorded enabled solution of the ground state magnetic structures of $M(NCS)_2$ using the method described in the Experimental and Results sections. Figures S8–S11 inclusive show expanded views of the Rietveld fits to the powder neutron diffraction data recorded for each material at their base temperatures.

Figure S8. Rietveld fit of the powder neutron diffraction pattern recorded on Bank 2 of WISH for $Mn(NCS)_2$ at 1.5 K between $Q = 0.48$ Å^{-1} and $Q = 4.0$ Å^{-1}, with $R_{wp} = 7.54\%$. Arrows lie directly above peaks arising from magnetically ordered $Mn(NCS)_2$, whilst asterisks lie directly above magnetic impurities and daggers lie directly above non-magnetic impurities. Inset shows an expansion of the fit between $Q = 0.50$ Å^{-1} and $Q = 1.67$ Å^{-1}.

Figure S9. Rietveld fit of the powder neutron diffraction pattern recorded on Bank 2 of GEM for $Fe(NCS)_2$ at 10 K between $Q = 0.50$ Å^{-1} and $Q = 4.0$ Å^{-1}, with $R_{wp} = 2.99\%$. Arrows lie directly above peaks arising from magnetically ordered $Fe(NCS)_2$. Inset shows an expansion of the fit between $Q = 0.50$ Å^{-1} and $Q = 1.90$ Å^{-1}.

Figure S10. Rietveld fit of the powder neutron diffraction pattern recorded on Bank 2 of WISH for $Co(NCS)_2$ at 1.5 K between $Q = 0.50$ Å^{-1} and $Q = 4.0$ Å^{-1}, with $R_{wp} = 4.06\%$. Arrows lie directly above peaks arising from magnetically ordered $Co(NCS)_2$, whilst asterisks lie directly above magnetic impurities. Inset shows an expansion of the fit between $Q = 0.50$ Å^{-1} and $Q = 1.75$ Å^{-1}.
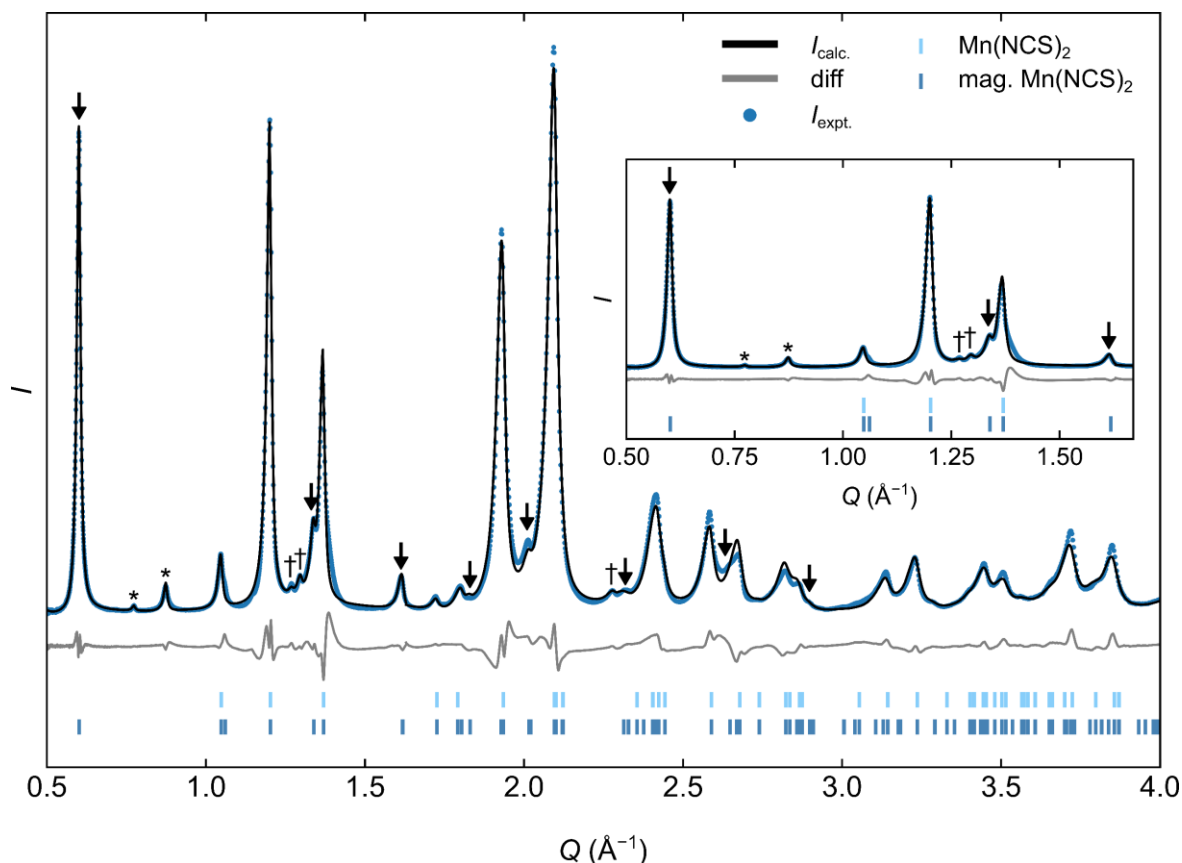
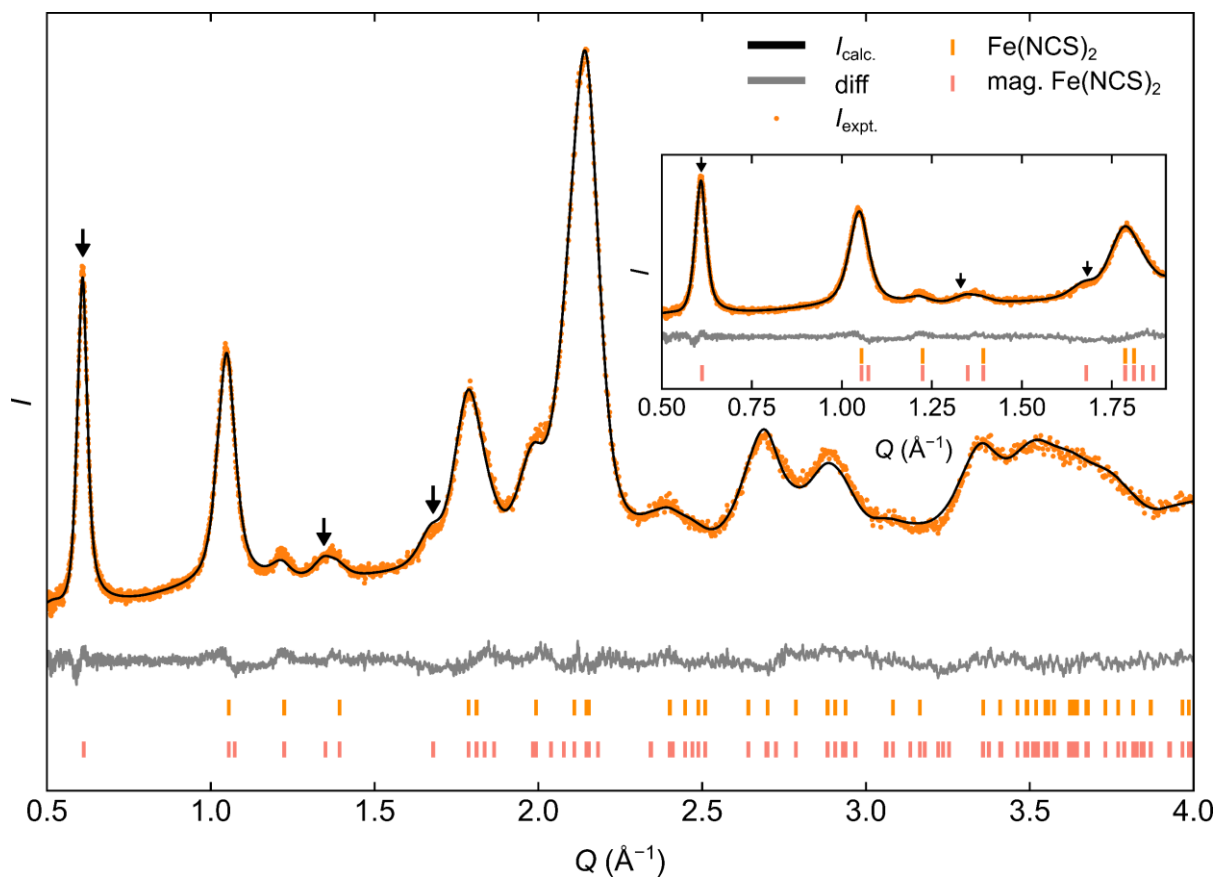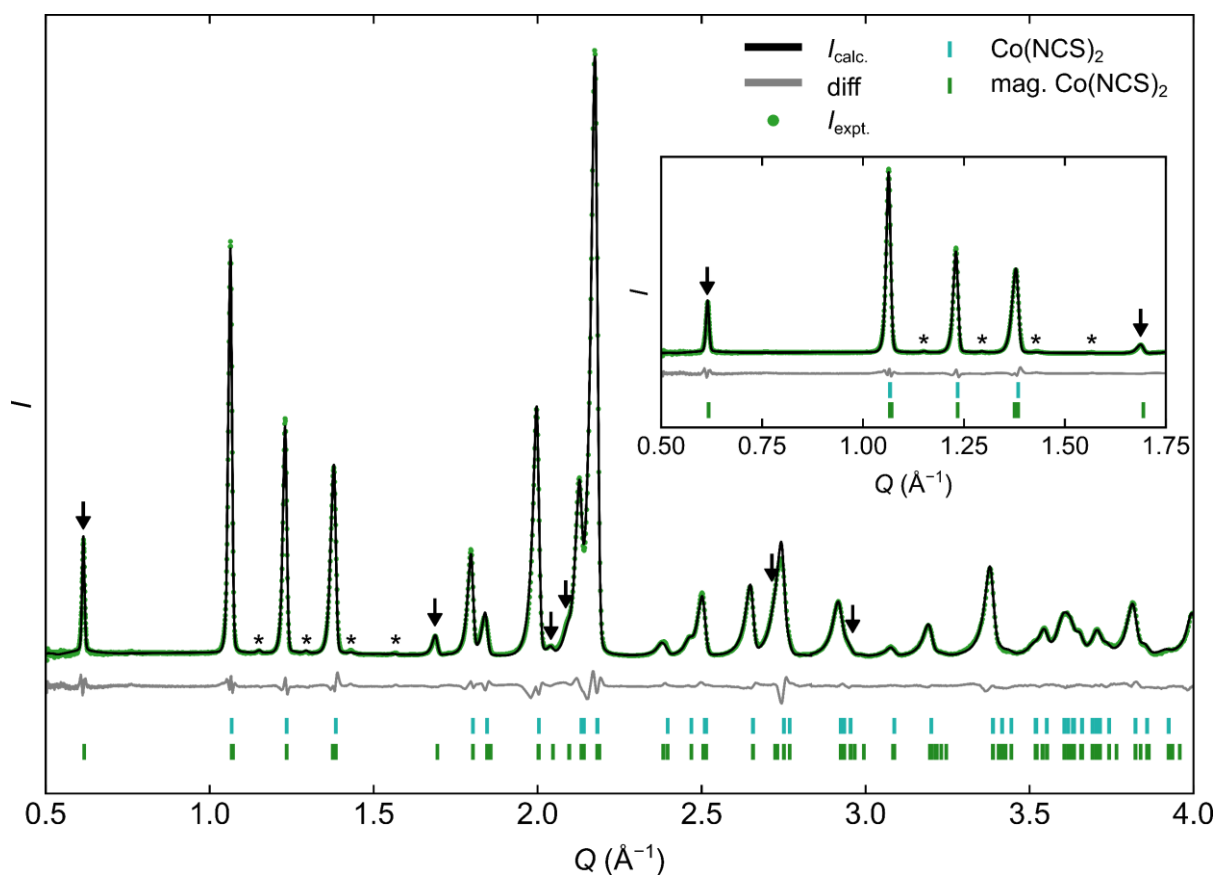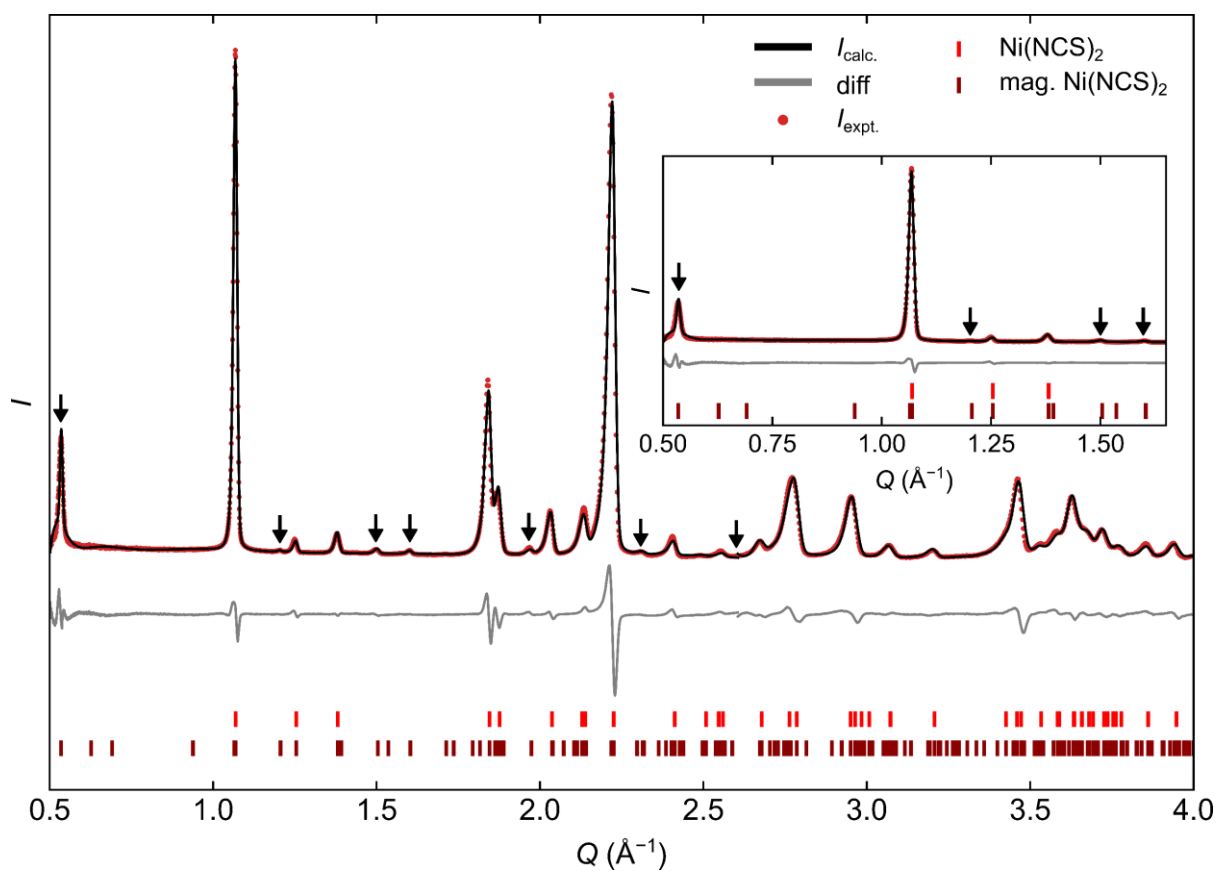**Figure S11.** Rietveld fit of the powder neutron diffraction pattern recorded on Bank 2 of WISH for $Ni(NCS)_2$ at 1.5 K between $Q = 0.50$ Å^{-1} and $Q = 4.0$ Å^{-1}, with $R_{wp} = 6.25\%$. Arrows lie directly above peaks arising from magnetically ordered $Ni(NCS)_2$. Inset shows an expansion of the fit between $Q = 0.50$ Å^{-1} and $Q = 1.65$ Å^{-1}.

7. Powder Neutron Diffraction Variable Temperature Results

In addition to the patterns recorded at base temperature, the variation in the powder neutron diffraction pattern of each material was recorded as a function of temperature. Rietveld refinements[2,3] of each diffraction pattern were performed using TOPAS Academic 6 structure refinement software.[4,5] These refinements produced the lattice parameters depicted in Figure S12. The bond angles and bond lengths obtained at base temperature are given in Table S1. The refined lattice parameters, atomic coordinates, ADPs and isotropic thermal displacement parameters are given in Tables S2–S6.
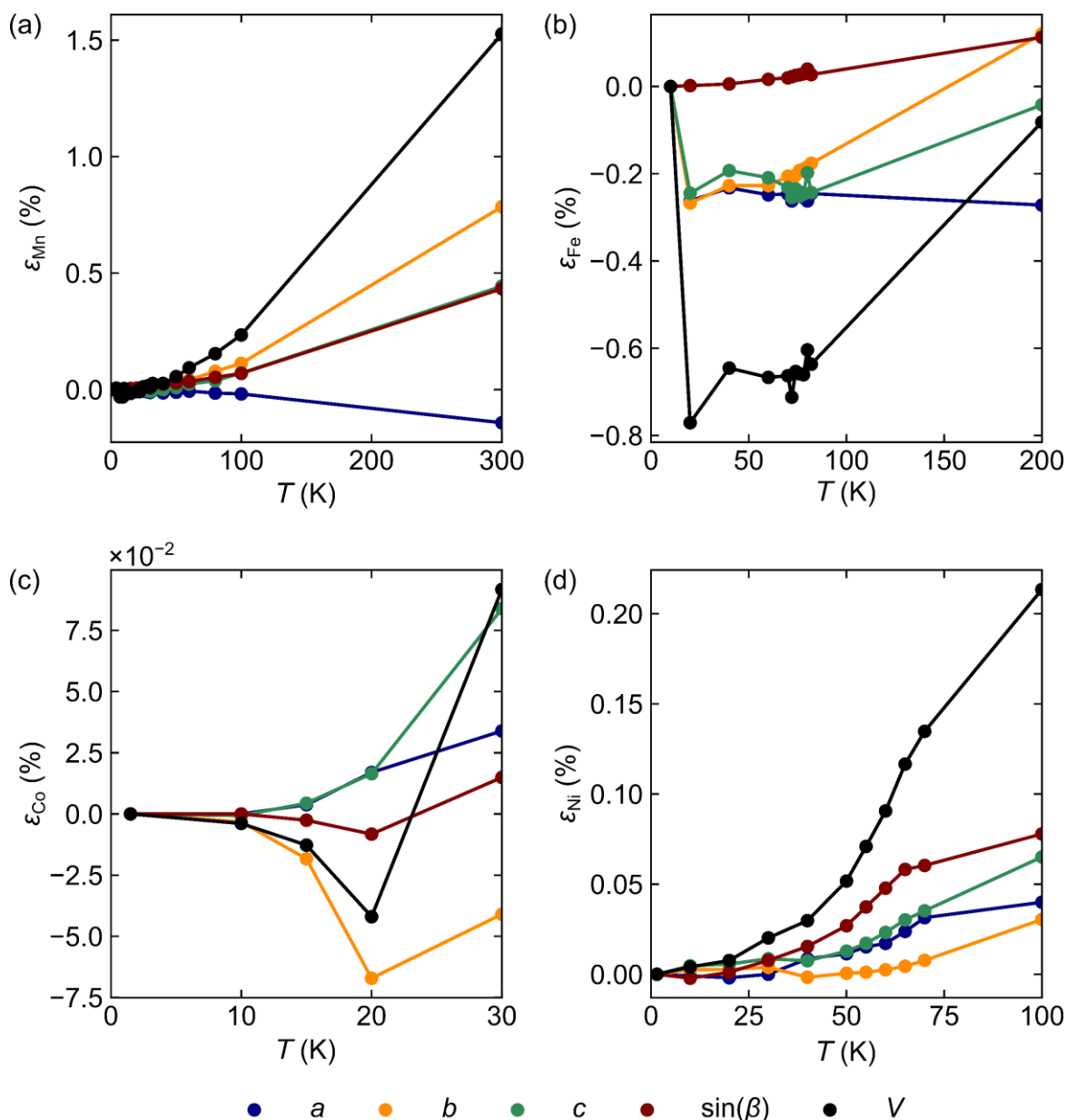
Figure S12. Temperature variation in strain in Rietveld-derived lattice parameters with for $M(NCS)_2$, M = Mn **(a)**; Fe **(b)**; Co **(c)** and Ni **(d)**. The strain in each parameter, p (p = a, b, c, $\sin(\beta)$, V), is calculated via $\varepsilon_M = \frac{p - p_{base}}{p_{base}}$, where p_{base} is the value of the lattice parameter at the base temperature—i.e. T = 1.5 K for $Mn(NCS)_2$, $Co(NCS)_2$ and $Ni(NCS)_2$ and T = 10 K for $Fe(NCS)_2$. These strains are expressed as percentages.

Table S1. Bond distances and bond angles derived from Rietveld-refined atomic coordinates and lattice parameters for $M(NCS)_2$ (M = Mn, Fe, Co, Ni) at base temperature: T = 1.5 K for $Mn(NCS)_2$, $Co(NCS)_2$ and $Ni(NCS)_2$ and T = 10 K for $Fe(NCS)_2$.

	Mn(NCS)$_2$	Fe(NCS)$_2$	Co(NCS)$_2$	Ni(NCS)$_2$
r_{M-N} (Å)	2.11846(7)	2.063(3)	2.02705(5)	1.97774(7)
θ_{M-N-C} (°)	166.3531(6)	162.62(10)	163.7661(7)	160.7094(9)
r_{M-S} (Å)	2.69556(6)	2.566(4)	2.55048(6)	2.48351(7)
θ_{M-S-M} (°)	92.133(3)	93.65(14)	93.281(3)	93.536(3)
θ_{M-S-C} (°)	103.0181(18)	100.83(12)	103.0691(16)	102.756(3)
r_{N-C} (Å)	1.24211(5)	1.178(3)	1.17665(4)	1.18854(5)
r_{S-C} (Å)	1.48187(6)	1.670(5)	1.58319(5)	1.59011(6)
θ_{N-C-S} (°)	174.7861(3)	175.92(14)	175.929(10)	178.692(10)

For $Mn(NCS)_2$, diffraction patterns were recorded at 1.5 K, 3.0 K, 4.0 K, 5.0 K, 6.0 K, 7.0 K, 8.0 K, 9.0 K, 10.0 K, 15.0 K, 20.0 K, 22.0 K, 24.0 K, 25.0 K, 26.0 K, 27.0 K, 28.0 K, 29.0 K, 30.0 K, 32.0 K, 40.0 K, 50.0 K, 60.0 K, 80.0 K, 100.0 K and 300.0 K.

For $Fe(NCS)_2$, diffraction patterns were recorded at 10.0 K, 20.0 K, 40.0 K, 60.0 K, 70.0 K, 72.0 K, 74.0 K, 76.0 K, 78.0 K, 80.0 K, 82.0 K and 200.0 K.

For $Co(NCS)_2$, diffraction patterns were recorded at 1.5 K, 10.0 K, 15.0 K, 20.0 K and 30.0 K.

For $Ni(NCS)_2$, diffraction patterns were recorded at 1.5 K, 10.0 K, 20.0 K, 30.0 K, 40.0 K, 50.0 K, 55.0 K, 60.0 K, 65.0 K, 70.0 K and 100.0 K.

Table S2. Refined atomic coordinates and lattice parameters for $Mn(NCS)_2$ at T = 1.5 K on Bank 2 of WISH. Estimated standard errors are given in parentheses.

Radiation Source	Neutrons		
Formula	$Mn(NCS)_2$		
M_r (g mol^{-1})	171.094		
Z	2		
R_{wp}	7.54		
Goodness of fit	0.299		
Crystal System	Monoclinic		
Space Group	$C2/m$		
a (Å)	10.8370(17)		
b (Å)	3.8824(6)		
c (Å)	6.2175(9)		
α (°)	90		
β (°)	105.348(2)		
γ (°)	90		
V (Å^3)	252.26(7)		
Atom	x	y	z
Mn	0	0	0
N	−0.1445(2)	0	0.1723(4)
C	−0.2465(4)	0	0.2278(6)
S	−0.3743(7)	0	0.2721(11)

Table S3. Refined atomic coordinates and lattice parameters for $Fe(NCS)_2$ at T = 10 K on Bank 2 of GEM. Estimated standard errors are given in parentheses.

Radiation Source	Neutrons		
Formula	$Fe(NCS)_2$		
M_r (g mol^{-1})	172.001		
Z	2		
R_{wp}	2.99		
Goodness of fit	2.97		
Crystal System	Monoclinic		
Space Group	$C2/m$		
a (Å)	10.630(16)		
b (Å)	3.742(6)		
c (Å)	6.168(10)		
α (°)	90		
β (°)	105.038(7)		
γ (°)	90		
V (Å^3)	237.0(6)		
Atom	X	y	z
Fe	0	0	0
N	−0.14037(13)	0	0.17658(18)
C	−0.24139(14)	0	0.2220(2)
S	−0.3897(3)	0	0.2668(4)

Table S4. Refined atomic coordinates and lattice parameters for Co(NCS)$_2$ at T = 1.5 K on Bank 2 of WISH. Estimated standard errors are given in parentheses.

Radiation Source	Neutrons		
Formula	Co(NCS)$_2$		
M_r (g mol^{-1})	175.089		
Z	2		
R_{wp}	4.06		
Goodness of fit	0.0718		
Crystal System	Monoclinic		
Space Group	$C2/m$		
a (Å)	10.6118(4)		
b (Å)	3.70869(11)		
c (Å)	6.13996(19)		
α (°)	90		
β (°)	106.4401(8)		
γ (°)	90		
V (Å^3)	231.763(13)		
Atom	X	y	z
Co	0	0	0
N	−0.13799(7)	0	0.17056(13)
C	−0.23820(11)	0	0.2171(2)
S	−0.3782(2)	0	0.2610(4)

Table S5. Refined atomic coordinates and lattice parameters for Ni(NCS)$_2$ at T = 1.5 K on Bank 2 of WISH. Estimated standard errors are given in parentheses.

Radiation Source	Neutrons		
Formula	Ni(NCS)$_2$		
M_r (g mol^{-1})	174.849		
Z	2		
R_{wp}	6.25		
Goodness of fit	0.376		
Crystal System	Monoclinic		
Space Group	$C2/m$		
a (Å)	10.5070(5)		
b (Å)	3.61889(5)		
c (Å)	6.16252(16)		
α (°)	90		
β (°)	107.509(3)		
γ (°)	90		
V (Å^3)	223.466(12)		
Atom	x	y	z
Ni	0	0	0
N	−0.1325(2)	0	0.1699(4)
C	−0.2367(3)	0	0.2085(5)
S	−0.3778(6)	0	0.2543(9)

Table S6. Refined atomic displacement parameters for each atom, X, in $M(NCS)_2$ ($X = M$, N, C, S). The same set of freely refining parameters was used for each atom in a given structure, with each compound having a unique set of parameters. Note that u_{12}, $u_{23} = 0$ for $Mn(NCS)_2$, $Co(NCS)_2$ and $Ni(NCS)_2$; the same isotropic thermal displacement parameter was used for all atoms in $Fe(NCS)_2$. Standard errors are given in parentheses.

M in $M(NCS)_2$	u_{11}	u_{22}	u_{33}	u_{13}
Mn	0.0049(12)	0.0101(12)	0.0285(13)	−0.0021(9)
Co	0.0108(4)	0.0115(3)	0.0209(4)	0.0079(4)
Ni	0.0070(7)	0.0056(6)	0.0248(8)	0.0112(6)

M in $M(NCS)_2$	B_{iso} (Å^2)
Fe	0.353(14)

8. References

(1)   Pawley, G. S. Unit-Cell Refinement from Powder Diffraction Scans. *J. Appl. Crystallogr.* **1981**, *14* (6), 357–361.

(2)   Rietveld, H. M. Line Profiles of Neutron Powder-Diffraction Peaks for Structure Refinement. *Acta Crystallogr.* **1967**, *22* (1), 151–152.

(3)   Rietveld, H. M. A Profile Refinement Method for Nuclear and Magnetic Structures. *J. Appl. Crystallogr.* **1969**, *2* (2), 65–71.

(4)   Coelho, A. TOPAS-Academic: General Profile and Structure Analysis Software for Powder Diffraction Data. Brisbane, Australia 2007.

(5)   Coelho, A. A. *TOPAS* and *TOPAS-Academic*: An Optimization Program Integrating Computer Algebra and Crystallographic Objects Written in C++. *J. Appl. Crystallogr.* **2018**, *51* (1), 210–218.